

Phase-Space Density Profiles in Scale-Free Cosmologies

Steffen R. Knollmann¹, Alexander Knebe¹ and Yehuda Hoffman²

¹*Astrophysikalisches Institut Potsdam, An der Sternwarte 16, 14482 Potsdam, Germany*

²*Racah Institute of Physics, Hebrew University, Jerusalem 91904, Israel*

25 March 2022

ABSTRACT

We use a set of high-resolution simulations of scale-free Einstein-de Sitter cosmologies to investigate the logarithmic slope of the phase-space density profile $Q(r) = \rho(r)/\sigma^3(r)$ of dark matter (DM) haloes. The initial conditions for the simulations are determined by a power law power spectrum of the form $P(k) \propto k^n$. We compute the $Q(r)$ profiles using the radial, tangential and full velocity dispersion, and the velocity anisotropy parameter, $\beta(r)$. We express $Q(r)$ as a single power-law $Q(r) \propto r^\alpha$ and derive a median slope α in each simulation and for each definition of Q . Our main findings are: 1. The various $Q(r)$ profiles follow a power law to a good approximation. 2. The slopes depend on the concentration parameter c of the DM haloes, where for $c \gtrsim 10$ the slopes steepen with rising concentration and for $c \lesssim 10$ the trend flattens and even turns around. 3. The asymptotic value of β as $r \rightarrow R_{\text{vir}}$ increases with the value of c . 4. In accordance with Zait et al. (2007) α_{rad} becomes more negative as the asymptotic value of β at the virial radius increases. 5. This introduces a weak dependence of the $Q(r)$ slopes on the slope of the power spectrum.

Key words: cosmology: theory — dark matter — methods: numerical

1 INTRODUCTION

For the density profile $\rho(r)$ of dark matter (DM) haloes a variety of empirical fitting formulae exist. The one applied mostly is the so-called NFW (Navarro et al. 1996, 1997) profile, which gives a fair description for haloes found in a wide range of N -body simulations. Recent studies though are hinting to use a different functional form for the density profile that differs from the usual NFW form mainly in the central regions (see, e.g. Navarro et al. 2004; Merritt et al. 2006), but common to all suggested profiles is the fact that they are not described by a simple power-law but rather require a smoothly changing logarithmic slope. It comes therefore as a surprise that the coarse-grained phase-space density¹ profile, calculated from the density- and the velocity dispersion profile $\sigma(r)$ as

$$Q(r) = \frac{\rho(r)}{\sigma^3(r)}, \quad (1)$$

very closely follows a *single* power-law $Q(r) \propto r^\alpha$ with $\alpha \approx -1.9$. This was first noted by Taylor & Navarro (2001) and has since been confirmed by many other works (e.g. Boylan-Kolchin & Ma 2004; Rasia et al. 2004; Ascasibar et al. 2004;

Austin et al. 2005; Dehnen & McLaughlin 2005; Hoffman et al. 2007; Ascasibar & Gottlöber 2008).

Different velocity dispersions have been used with equation 1, generally the radial velocity dispersion $\sigma_{\text{rad}}(r)$ is used, but also the total velocity dispersion $\sigma_{\text{tot}}(r)$ has been employed. Both lead to separate definitions for Q that nevertheless can be well fitted with a single power-law, albeit marginal differences in the slopes (Dehnen & McLaughlin 2005; Faltenbacher et al. 2007; Ascasibar & Gottlöber 2008), see also the discussion in Zait et al. (2007).

The power law phase-space density profile has been found mostly in simulations of structure formation in the standard model of cosmology, namely the flat Λ CDM model. It is not known how general its behaviour in other cosmologies is and the dynamical origin of the power-law is not yet understood. However, the structure of (spherical) haloes in equilibrium obeys the (spherical) Jeans equation which relates the density profile, the phase-space density profile and the velocity anisotropy parameter β (to be defined below). As mentioned above, the universality of the density profile is well-established across a large variety of cosmological models. The description of the phase-space density profiles as a single power-law, however, is not that well checked.

Hence we aim here at studying the (phase-space) structure of DM haloes in different cosmogonies, in particular scale-free Einstein-de Sitter cosmologies with varying spectral index n , to explicitly probe universality of the phase-space profile. We use the numerical simulations of

¹ See, e.g., Dehnen & McLaughlin (2005) for clarifications about the applicability of the term ‘phase-space density’, as the term is commonly used, however, we will continue to refer to $Q(r)$ as the phase-space density profile.

Table 1. Simulation details.

Name	Type	B	A/σ_8	Ω_m	Ω_Λ	N	N_h
512-0.50	$n = -0.50$	1	0.0358	1.0	0.0	512^3	186
512-1.50	$n = -1.50$	1	0.0215	1.0	0.0	512^3	106
512-2.25	$n = -2.25$	1	0.0109	1.0	0.0	512^3	61
512-2.50	$n = -2.50$	1	0.0076	1.0	0.0	512^3	34
512-2.75	$n = -2.75$	1	0.0046	1.0	0.0	512^3	14
256-B50	Λ CDM	50	0.9	0.3	0.7	256^3	19

Summary of the simulations. The first column simply assigns a unique label used throughout the paper while the second column specifies the model. B refers to the side length of the simulation box. A (σ_8) is the normalisation of the input power spectrum used to generate the initial conditions. Ω_m and Ω_Λ describe the background cosmology. N gives the number of particles in the model and N_h the number of haloes used for the analysis.

Knollmann et al. (2008) who studied the structure of haloes in pure DM flat cosmologies with a primordial power spectrum of the form $P(k) \propto k^n$, finding the equilibrium haloes to be well described by a universal density profile. Scale-free models provide a clean probe of the possible dependence of the structure of DM halos on the primordial initial conditions. This provides insight to the concordance Λ CDM model in the sense that the power spectrum for this cosmology exhibits a varying slope depending on the scale.

We shall further investigate the behaviour of the phase-space density profile with different components of the total velocity dispersion σ_{tot} , namely the radial and tangential dispersions. Given the close connection between the $Q(r)$ power law and the velocity anisotropy (Zait et al. 2007), expressed by the β parameter, the β profile of the DM haloes is to be explicitly studied. The paper is organized as follows. The numerical experiments are briefly discussed in §2. The fitting of the phase-space density profile is described in §3 and the results are presented in §4. The paper concludes with a summary and discussion in §5.

2 NUMERICAL EXPERIMENTS

We base our analysis on the simulations described in Knollmann et al. (2008). Those simulations are set up according to a power spectrum of the initial density perturbations of the form

$$P(k) \propto k^n. \quad (2)$$

Five different models have been simulated with $n = -0.50, -1.50, -2.25, -2.50$ and -2.75 . The simulations were performed with the parallel N -body code GADGET2 (Springel 2005) following the evolution of 512^3 dark matter particles. The final stage of each run is chosen in such a way that M_* – the typical collapsing mass – reaches the same value for all choices of n (for a more detailed description see Knollmann et al. 2008).

We then employ the MPI version of the AMIGA Halo Finder² (AHF, successor of MHF introduced by Gill et al. (2004)) to identify haloes and to compute their radial and

integral properties. The radial properties are calculated in logarithmic bins in r and only those bins which are converged according to the criteria presented in Power et al. (2003) are retained for the analysis. We further restrict our sample of haloes to those having a mass M in the range $[0.75M_*, 1.5M_*]$ where a typical M_* halo is resolved with 4.2×10^4 particles.

Also, we require the haloes to be relaxed, for which we have used the displacement Δ_r of the centre of mass of all material inside the virial radius with respect to the potential centre normalized to the virial radius

$$\Delta_r = |\mathbf{r}_{\text{cm}} - \mathbf{r}_{\text{cen}}|/r_{\text{vir}}. \quad (3)$$

For inclusion in the sample, we require $\Delta_r \leq 0.05$, employing a more conservative value than proposed by other recent studies (e.g. Neto et al. 2007).

For comparison we also use the results of a “standard” Λ CDM simulation analysed at $z = 0$ whose particulars are described in detail elsewhere (Power et al. in prep.). Using that simulation we define a halo sample labelled 256-B50 including all haloes resolved with more than 3.15×10^4 particles (corresponding to a halo of mass $0.75M_*$ in the scale-free simulations) and being relaxed according to the same “off-centre” criterion alluded to above. A summary of the simulation parameters and the halo samples is given in table 1.

3 PHASE-SPACE DENSITY PROFILES

The evaluation of the phase-space density as defined by equation 1 requires the (total) velocity dispersion $\sigma_{\text{tot}}(r)$ at the radius r , which is calculated as

$$\sigma_{\text{tot}}^2(r) = \frac{1}{N_{\text{sh}} - 1} \sum_{i=1}^{N_{\text{sh}}} |\mathbf{v}_{\text{tot},i} - \langle \mathbf{v}_{\text{tot}} \rangle|^2 \quad (4)$$

where the sum extends over the N_{sh} particles contained in a shell with radius r . With $\mathbf{v}_{\text{tot},i}$ and $\langle \mathbf{v}_{\text{tot}} \rangle$ we refer to the velocity of the i th particle and the average velocity within the shell, respectively. For the calculation of the radial phase-space density $Q_{\text{rad}}(r)$ we project the 3D velocity $\mathbf{v}_{\text{tot},i}$ onto the radial direction and use only the radial component with equation 4, respectively. With these two velocity dispersions we can obtain the tangential velocity dispersion σ_{tan} by using the relation

$$\sigma_{\text{tan}}^2 = \sigma_{\text{tot}}^2 - \sigma_{\text{rad}}^2 \quad (5)$$

for the calculation of the tangential phase-space density profile $Q_{\text{tan}}(r)$.

3.1 Normalization

For each halo we normalize the radius r by r_2 and the Q profile by $Q_2 \equiv Q(r_2)$, where r_2 is the radius at which the density profile has a slope of -2 .³ We find this “scaling radius” in a non-parametric way by locating the maximum of $r^2\rho(r)$. Having identified r_2 for each halo and representing

² AMIGA is freely available for download at <http://www.aip.de/People/AKnebe/AMIGA/>

³ In the case of an NFW profile r_2 corresponds to the scale radius r_s .

its Q -profile with a cubic spline, Q_2 is then readily available as the evaluation of the spline interpolation at r_2 .

Additionally, we define for each halo a concentration parameter c as

$$c = \frac{r_{\text{vir}}}{r_2} \quad (6)$$

where r_{vir} is the virial radius defined via $3M(< r_{\text{vir}}) = 4\pi\Delta_{\text{vir}}\rho_b r_{\text{vir}}^3$ with ρ_b being the cosmic background density and $\Delta_{\text{vir}}=178$ (340) for the scale-free (Λ CDM) model. The concentration c has been found to be a distinguishing quantity between haloes from different scale-free models, with haloes forming in a shallower cosmology being more concentrated (cf. Knollmann et al. 2008).

3.2 Fitting

The normalized Q -profiles of each halo are fitted by a single power-law

$$q(r; \alpha) = Q_2 \left(\frac{r}{r_2} \right)^\alpha \quad (7)$$

by minimizing the quantity

$$\chi^2(\alpha) = \sum_i \left(\frac{Q(r_i) - q(r_i; \alpha)}{0.1 \cdot Q(r_i)} \right)^2. \quad (8)$$

Note that due to the choice of our normalization we have only the slope α as a free parameter.

4 RESULTS

In this section, we will describe our results, starting in subsection 4.1 with the power-law nature of the phase-space density profiles. We will then, in subsection 4.2, focus on the individual slopes probing for the generality of the slopes and on what quantities they depend. We will then shortly investigate the relation between the three different Q profiles in subsection 4.3, before finally focussing on the velocity anisotropy profiles in subsection 4.4.

4.1 Phase-space density profiles

In figure 1 the different Q -profiles (i.e. radial, tangential and total) are shown in the normalization described above alongside the best-fitting power-laws for the respective simulation (i.e. the power law as given by the median of all α 's for a given model and Q , respectively). The median slopes used to draw the power laws are given in table 2, which we will describe later in greater detail.

Furthermore, to avoid crowding, the profiles for the different simulations are offset to one another by factors given in the key. For all profiles the power law structure is quite convincing – irrespective of the simulation. We also investigated the residuals of fits (though not shown here), finding the average deviation per degree of freedom to be on the order of 40 per cent, further strengthening the single power law fit to be a reasonable choice. In the next subsection, we will use the slopes derived for each halo.

4.2 The universality of the slope

It is known that haloes formed in runs with different spectral index n favour different concentrations⁴ but are otherwise compatible with a universal density slope (cf. Knollmann et al. 2008). We therefore investigate the slopes α of individual haloes as a function of their concentration c . This is shown in figure 2, where the left (middle, right) panel corresponds to the radial (angular, total) Q profile. Additionally, the simulations the haloes originate from are symbolised by different colours (see the caption of figure 2 for a description, we will use those symbols and colours for the remainder of the paper). The information contained in figure 2 is hence two-fold: a) the connection of α to the model⁵ is visualised by the colour and b) the dependence on the concentration is encoded on the abscissa.

To investigate those two effects more closely – and to understand which is the more fundamental dependence – we will probe the relations separately, looking for the one yielding the smaller scatter. To this extent, we bin all haloes from the scale-free models in c , regardless of their model identity; the medians and the upper and lower quartiles in the bins are shown in the left panel of figure 3. We then use the median α in each model to construct the right panel of figure 3, showing the trend for $\alpha - n$. The curves for the different definitions of Q are offset to one another to avoid crowding. The median values and the upper and lower quartiles are also given in tables 2 and 3, respectively.

We first note that, ignoring the model identity and combining all haloes, a clear, yet noisy, trend can be observed: For haloes with a concentration $c \gtrsim 10$ the Q profiles steepen with rising c , whereas a flattening of the $\alpha - c$ curve occurs for concentrations $c \lesssim 10$. This is reflected in the $\alpha - n$ relation, for flat n models, we find steeper Q profiles, with the $n = -2.75$ model, however, showing a steeper median α than the $n = -2.50$ and $n = -2.25$ models. We also note that neither the $\alpha - c$ nor the $\alpha - n$ is clearly preferred as the fundamental relation, both have a comparable scatter in α , with maybe the former slightly favoured.

In order to check whether our results are an artifact of the fitting procedure we performed three additional tests: a) we fitted the Q -profiles confining the radial range to $0.1 < r/r_2 < 10$ (i.e. the fitting has been performed over a fixed dynamical range for all the haloes of all the different models considered here), b) we subdivided the sample of each model into a low and high concentration bin and calculated the median α in those two bins for each model, and c) we calculated the reduced χ^2 for each individual halo fit and inspected its distribution. All these checks indicate that the results seen and presented in figures 2 and 3 are stable.

For test a) we recover a similar distribution as shown in figure 2. The second test traces the global trend shown in the left panel of figure 3, with the $n = -0.50$ and $n = -1.50$ models showing a steeper Q -profile for the high concentration subsample, whereas the $n = -2.25$ shows a similar α

⁴ This is already apparent in figure 1: the Q -profiles are plotted out to the virial radius and hence the final point is a direct measure of concentration for our choice of units.

⁵ This means effectively a dependence on the spectral index n of the power spectrum of initial density perturbations.

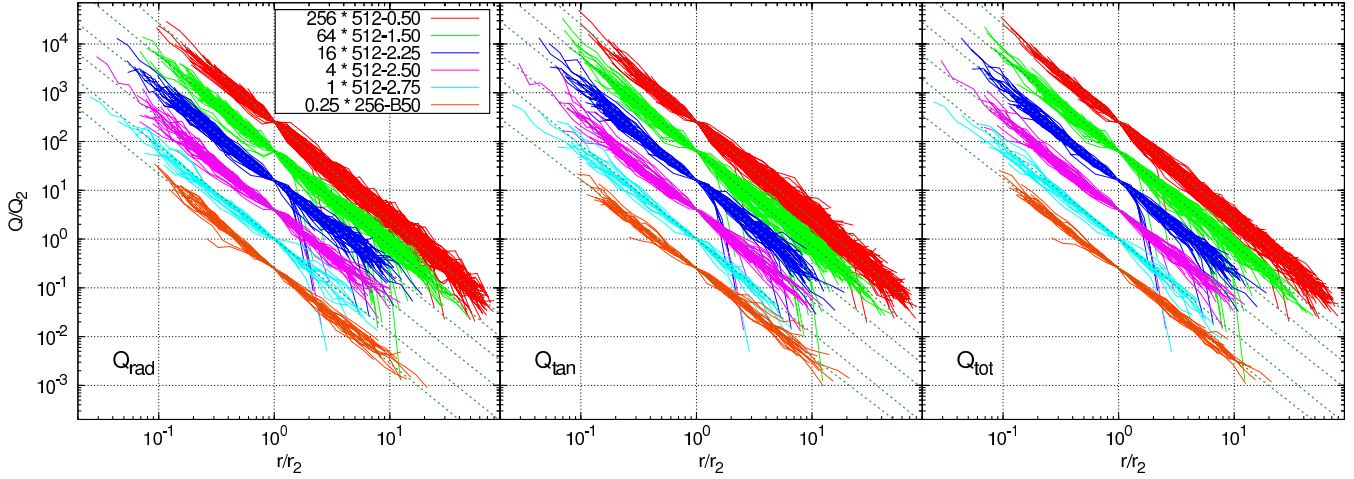


Figure 1. Phase-space density profiles $Q(r)$ for our sample of haloes (radial, tangential, and total velocity dispersions are used in the left, middle, and right panel). The profiles of the different simulations are shifted on the y -axis for clarity, the factor by which they are shifted is given in the key. For each simulation we also show the best-fitting r^α power-law, as given by the median value of α within the simulation; cf. table 2 for the actual values.

Table 2. Median slopes of the phase-space density profiles depending on the model.

Model	α_{rad}	α_{tan}	α_{tot}
512-0.50	$-2.02_{-2.08}^{-1.97}$	$-2.00_{-2.06}^{-1.91}$	$-1.99_{-2.04}^{-1.93}$
512-1.50	$-1.95_{-2.02}^{-1.88}$	$-1.94_{-2.02}^{-1.83}$	$-1.92_{-2.00}^{-1.86}$
512-2.25	$-1.89_{-1.98}^{-1.82}$	$-1.92_{-2.02}^{-1.86}$	$-1.90_{-1.99}^{-1.86}$
512-2.50	$-1.89_{-1.93}^{-1.82}$	$-1.87_{-1.93}^{-1.79}$	$-1.87_{-1.92}^{-1.83}$
512-2.75	$-1.91_{-1.94}^{-1.83}$	$-1.92_{-2.02}^{-1.84}$	$-1.93_{-1.99}^{-1.82}$
256-B50	$-1.94_{-1.98}^{-1.87}$	$-1.81_{-1.84}^{-1.75}$	$-1.85_{-1.87}^{-1.82}$

Table 3. Median slopes of the phase-space density profiles of the scale-free haloes depending on the concentration.

c	α_{rad}	α_{tan}	α_{tot}
5.05 $^{6.20}_{3.69}$	$-1.92_{-1.99}^{-1.82}$	$-1.93_{-2.07}^{-1.86}$	$-1.92_{-2.02}^{-1.85}$
9.55 $^{10.83}_{8.34}$	$-1.92_{-2.02}^{-1.86}$	$-1.90_{-1.98}^{-1.78}$	$-1.91_{-1.93}^{-1.84}$
16.67 $^{19.24}_{14.46}$	$-1.95_{-2.00}^{-1.89}$	$-1.91_{-1.97}^{-1.83}$	$-1.90_{-1.95}^{-1.87}$
33.21 $^{39.61}_{27.81}$	$-1.98_{-2.05}^{-1.94}$	$-1.99_{-2.03}^{-1.91}$	$-1.98_{-2.02}^{-1.93}$
57.55 $^{64.01}_{51.00}$	$-2.03_{-2.08}^{-2.00}$	$-2.04_{-2.09}^{-1.99}$	$-2.03_{-2.07}^{-1.99}$

in both bins and the steeper models show a steeper α for the low concentration bin, e.g. the opposite of what is found in the flatter models. It should be noted though, that due to the low numbers of haloes available in the steep models ($n < -2.25$, cf. table 1), this might just be a statistical effect. Lastly, the probability distributions of χ^2_{rad} , χ^2_{tan} , and χ^2_{tot} (not shown here though) confirm that all profiles are fitted equally well with the assumption of a single power-law, with the relative deviations per degree of freedom of the order of 40 per cent.

4.3 The relation between the different Q profiles

We will now investigate the relation of the different Q profiles. In agreement with previous studies (e.g. Dehnen &

McLaughlin 2005; Ascasibar & Gottlöber 2008) we find Q_{rad} to be steeper than Q_{tot} in our Λ CDM sample, i.e. $(\alpha_{\text{rad}}/\alpha_{\text{tot}})_{\Lambda\text{CDM}} \approx 1.05$. The scale-free simulations show at best a very marginal trend of this kind: The slopes of the radial and total Q -profiles for a given model tend to be much less different, i.e. $(\alpha_r/\alpha_{\text{tot}})_{\text{scale-free}} \approx 1.01$. However, the slope for a given Q -profile appears to change across models, namely to drop with increasing spectral index n (shown in the right panel of 3), with the notable exception of the 512-2.75 model which favours steeper Q profiles than the 512-2.50 model. As we have shown above, this is also seen as a $\alpha - c$ dependence, namely the slope of the Q profiles first rises with decreasing concentration c until $c \approx 10$, from where on the trend flattens and even turns around; this is shown in the left panel of figure 3.

Ascasibar & Gottlöber (2008) were the first to point out that not only Q_{rad} and Q_{tot} are single power-laws, but also Q_{tan} . They further showed that its slope is shallower than the slope Q_{tot} basing their findings on a suite of simulations of the concordance Λ CDM cosmology. We confirm this relation for the haloes in the (concordance) 256-B50 sample; we further find a single power-law to be a fair description of the Q_{tan} profile in the scale-free samples. However, in the scale-free sample α_{tan} tends to be slightly steeper than α_{tot} , but still shallower than α_{rad} .

4.4 The velocity anisotropy of scale-free haloes

Given the universal density profile the difference between the power law slopes of the different $Q(r)$ profiles implies that the anisotropy β of the velocity dispersion, given as

$$\beta = 1 - \frac{\sigma_{\text{tan}}^2}{2\sigma_{\text{rad}}^2} \quad (9)$$

is not constant. We investigate this in figure 4, showing in the left panel the mean $\beta(r)$ profiles of the different models. This shows an agreement of all profiles for $r \lesssim r_2$ but a dependence on the model in the outer part of the haloes. In the middle and right panel we now focus on the value

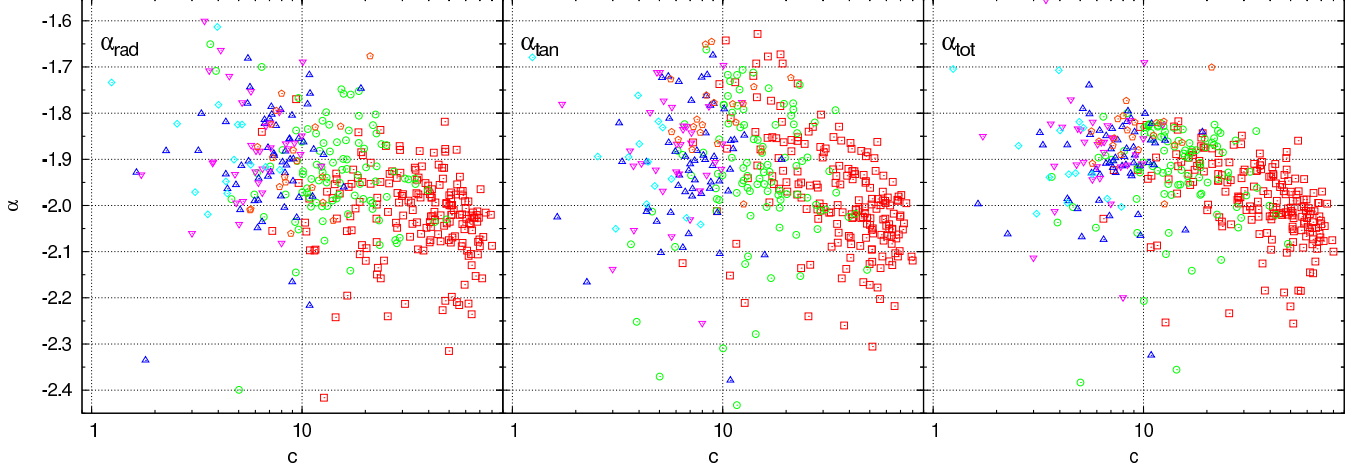


Figure 2. In this figure we show the derived slopes α of each halo versus its concentration $c = c_{\text{vir}}/r_2$. Each panel corresponds to using a different velocity dispersions to calculate $Q(r)$ (see equation 1), the results for $Q_{\text{rad}}(r)$ ($Q_{\text{tan}}(r)$, $Q_{\text{tot}}(r)$) are shown in the left (middle, right) column. The haloes are colour coded according to the model they correspond to: red $n = -0.50$ (open boxes), green $n = -1.50$ (open circles), blue $n = -2.25$ (open upright triangles), magenta $n = -2.50$ (open downright triangles), cyan $n = -2.75$ (open diamonds) and for comparison haloes from a Λ CDM simulation are shown in orange (open pentagons).

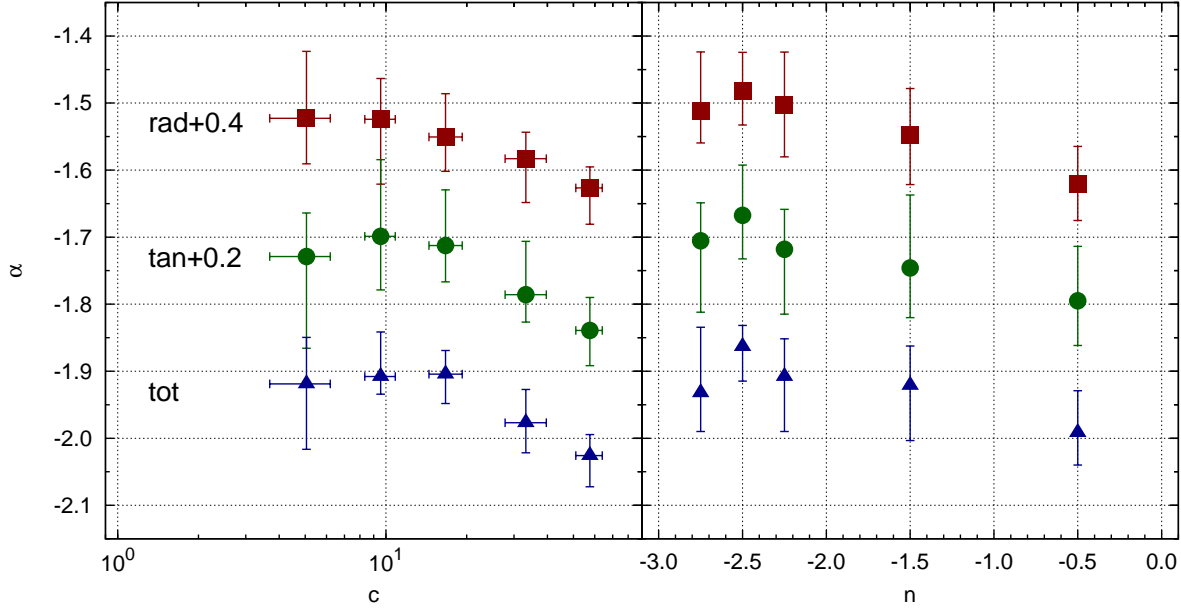


Figure 3. In this figure we investigate the relation of the slope α of the phase-space density profiles to the concentration c (left panel) and the spectral index n of the model (right panel). For clarity, the points corresponding to the tangential (dark green filled circles) and radial (dark red filled squares) Q -profile are offset to the ones corresponding to the total (dark blue filled triangles) Q -profile by 0.2 and 0.4, respectively. In the left panel we have binned the $\alpha - c$ distribution shown in figure 2 in c regardless of n , whereas in the right panel we combine the slopes of all haloes within one model regardless of the concentration (see also tables 2 and 3). We show the median and the lower and upper quartiles of each bin.

of the β profile at the virial radius and check for how it correlates with the slope of the radial Q profile α_{rad} and the concentration c , respectively.

We see a trend for $\beta(r_{\text{vir}})$ to become larger for a steeper radial Q profile, which also translates into a trend with c , namely, the larger the concentration the larger becomes $\beta(r_{\text{vir}})$; this is shown in the right-most panel of figure 4.

Recalling equation 9, we see that a larger $\beta(r_{\text{vir}})$ means that the total velocity dispersion becomes more radial. The $\beta(r_{\text{vir}}) - \alpha_{\text{rad}}$ trend we observe agrees with the findings of Zait et al. (2007) who calculated the β profile given the density profile and a power law Q_{rad} profile. They showed that a more negative α_{rad} implies a larger β for $r > r_2$, which means that the total velocity dispersion is more radial.

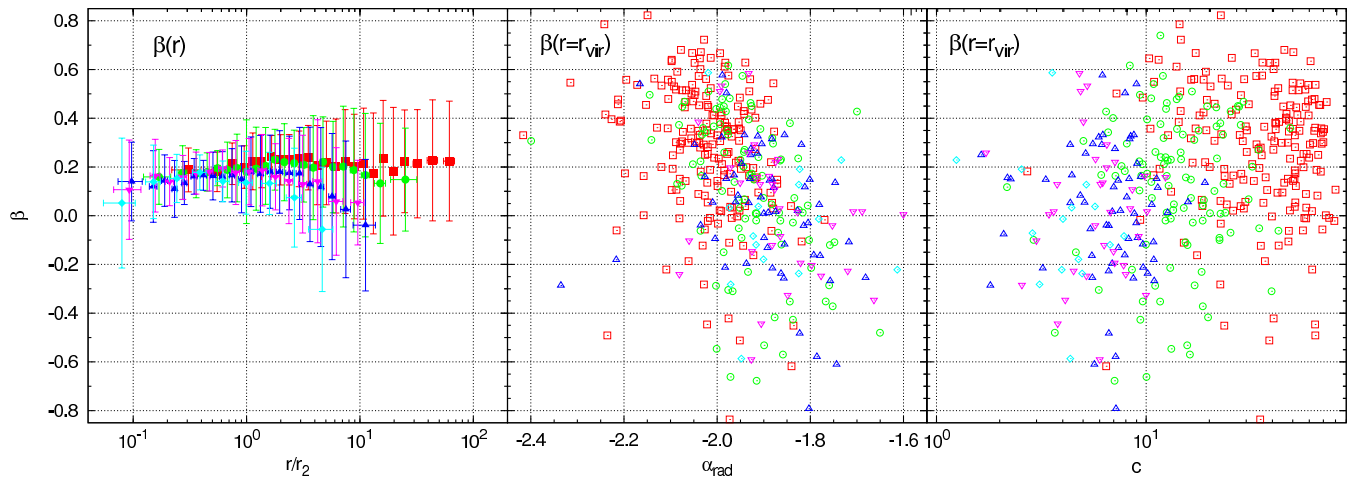


Figure 4. In the left panel, we show the mean β profile in each simulation, using the same colour coding as described in figure 2. Note that the last point corresponds to value of β at the virial radius. The middle panel gives the value of the anisotropy profile at the virial radius, $\beta(r_{\text{vir}})$, as a function of the slope of the radial Q -profile, α_{rad} . In the right panel the distribution of $\beta(r_{\text{vir}})$ as a function of the concentration is shown.

5 SUMMARY & DISCUSSION

We have analysed five high-resolution simulations of scale-free cosmologies and investigated the logarithmic slope α of the radial, angular and total phase-space density profiles $Q(r) = \rho(r)/\sigma^3(r)$ when fitted by a single power-law $Q(r) \propto r^\alpha$. Additionally, we used a halo sample drawn from a Λ CDM simulation as a control sample to verify our analysis procedure and reproduced previous results.

Focussing on a well-defined sample of haloes in each scale-free simulation, chosen to be in a comparable dynamical state, we derived the slopes α_{rad} , α_{tan} and α_{tot} for each halo and computed the median slopes in each simulation. We found that the slopes for the three definitions of the phase-space density profile Q vary between the models, namely Q becomes shallower with steeper spectral index n of the initial power spectrum $P(k) \propto k^n$, with the exception of the 512-2.75 model, which shows flatter Q profiles than found in the 512-2.50 model. We also find a trend for α to first become flatter with decreasing concentration; this trend flattens at $c \approx 10$ and even turns around for the tangential and total Q profiles. This is connected to previous findings showing a correlation between the power spectrum index n and the concentration c .

But how can the $n - c$ relation affect the $Q(r)$ profiles? The scaled density profiles appear to follow a universal form, independent of the cosmological model (see e.g. Navarro et al. 1996, 1997, 2004); in particular this has been shown explicitly for the models studied here (Knollmann et al. 2008). The dependence on the cosmological model (i.e. the slope of the power spectrum of initial density perturbations) is introduced via the concentration parameter, and thereby by the dependence of the β profile on the model. The Jeans equation, which dictates the structure of spherical DM haloes in equilibrium, relates the density, phase space density and the velocity anisotropy profiles (e.g. Zait et al. 2007, and references therein). Zait et al. showed that for a given density profile a more radial velocity dispersion at the outer parts of a halo implies a more negative α_{rad} ,

which is precisely what we find and have shown in figure 4. It is hence interesting to note that, even though the density profile follows a universal form, the β -profile does not, but rather depends on the concentration (Knollmann et al. 2008).

Summarizing past and present results the following conclusions can be drawn about DM haloes in scale-free cosmologies. The density profile shows a universal profile, upon an appropriate scaling, but the concentration parameter depends on the power spectrum index n (Knollmann et al. 2008). Here it has been found the phase-space density profile obeys a power law. The slope of its power law depends on whether the phase-space is defined in terms of the radial, tangential or the full velocity dispersion. Furthermore, the slopes depends on the shape of the power spectrum. Also, the velocity anisotropy at R_{vir} depends strongly on the power spectrum index.

The main problem addressed here is the universality of the phase-space density profile, and a mixed answer has been found. On the one hand it has been very robustly shown that indeed a power law profile provides a good fit in all models considered here. Yet, the power law slope α has been found to vary with power spectrum index n . Given our lack of understanding of the origin of the phase-space density power law it is interesting to trace the reason for the dependence of the slopes α on n . It has been shown here that at least part of that dependence is attributed to the concentration parameter variation with n . However, it is unclear whether there is a direct dependence of the slope α on n . This can be tested by comparing the slope and n relation for a subsample of haloes of different models with the same value of the concentration parameter. Regrettably, the sample of haloes used in the present work is too small to provide a clear answer.

ACKNOWLEDGEMENTS

SRK and AK acknowledge funding through the Emmy Noether Programme by the DFG (KN 755/1). Simulations and the analysis have been performed on the sanssouci and luise cluster at the AIP, except the 256-B50 which was performed on the Green machine at the Centre for Astrophysics and Supercomputing at Swinburne University. We thank Chris Power for providing us the snapshots.

REFERENCES

- Ascasibar Y., Gottlöber S., 2008, MNRAS, 386, 2022
Ascasibar Y., Yepes G., Gottlöber S., Müller V., 2004, MNRAS, 352, 1109
Austin C. G., Williams L. L. R., Barnes E. I., Babul A., Dalcanton J. J., 2005, ApJ, 634, 756
Boylan-Kolchin M., Ma C.-P., 2004, MNRAS, 349, 1117
Dehnen W., McLaughlin D. E., 2005, MNRAS, 363, 1057
Faltenbacher A., Hoffman Y., Gottlöber S., Yepes G., 2007, MNRAS, 376, 1327
Gill S. P. D., Knebe A., Gibson B. K., 2004, MNRAS, 351, 399
Hoffman Y., Romano-Díaz E., Shlosman I., Heller C., 2007, ApJ, 671, 1108
Knollmann S. R., Power C., Knebe A., 2008, MNRAS, 385, 545
Merritt D., Graham A. W., Moore B., Diemand J., Terzić B., 2006, AJ, 132, 2685
Navarro J. F., Frenk C. S., White S. D. M., 1996, ApJ, 462, 563
Navarro J. F., Frenk C. S., White S. D. M., 1997, ApJ, 490, 493
Navarro J. F., Hayashi E., Power C., Jenkins A. R., Frenk C. S., White S. D. M., Springel V., Stadel J., Quinn T. R., 2004, MNRAS, 349, 1039
Neto A. F., Gao L., Bett P., Cole S., Navarro J. F., Frenk C. S., White S. D. M., Springel V., Jenkins A., 2007, MNRAS, 381, 1450
Power C., Navarro J. F., Jenkins A., Frenk C. S., White S. D. M., Springel V., Stadel J., Quinn T., 2003, MNRAS, 338, 14
Rasia E., Tormen G., Moscardini L., 2004, MNRAS, 351, 237
Springel V., 2005, MNRAS, 364, 1105
Taylor J. E., Navarro J. F., 2001, ApJ, 563, 483
Zait A., Hoffman Y., Shlosman I., 2007, ArXiv e-prints, 711